Journal of Molecular Structure 1180 (2019) 455–461

Contents lists available at ScienceDirect

Journal of Molecular Structure

journal homepage: http://www.elsevier.com/locate/molstruc

Hydrophobic pocket docking, double-proton prototropic tautomerism in contradiction to single-proton transfer in thione ⇔thiol Schiff base with triazole-thione moiety: Green synthesis, XRD and DFT-analysis

Mohamed Reda Aouad [a], Mouslim Messali [a], Nadjet Rezki [a, b], Musa A. Said [a], Dieter Lentz [c], Lana Zubaydi [d], Ismail Warad [e, *]

[a] Department of Chemistry, Taibah University, 30002 Al-Madina Al-Mounawara, Saudi Arabia
[b] University of Sciences and Technology Mohamed Boudiaf, BP 1505, Oran, El M Nouar, Algeria
[c] Institut für Chemie und Biochemie, Anorganische Chemie, Freie Universität Berlin, Fabeckstr. 34-36, 14195 Berlin, Germany
[d] College of Pharmacy, An-Najah National University, P.O. Box 7, Nablus, Palestine
[e] Department of Chemistry, Science College, An-Najah National University, P.O. Box 7, Nablus, Palestine

ARTICLE INFO

Article history:
Received 16 October 2018
Received in revised form
4 December 2018
Accepted 4 December 2018
Available online 7 December 2018

Keywords:
Triazole
Prototropic tautomerism
Docking
XRD
DFT

ABSTRACT

In the present study, an eco-friendly and efficient microwave-assisted synthesis of the (*E*)-4-((3,4-difluorobenzylidene)amino)-2,4-dihydro-5-methyl-3*H*-1,2,4-triazole-3-thione Schiff base ligand was described. XRD-single crystal analysis reflected the molecule occurs in an *exo*-thione tautomeric form in solid state. Therefore, gaseous-phase prototropic thione thiol tautomerism occurrence probability *via* single-proton intramigration and push/pull protons self-assemble double proton transfer exchange was DFT-computed. The newly designed thione-tautomer was well-characterized by MS, FT-IR, CHN-EA, ^{19}F, ^{1}H, ^{13}C NMR, and XRD analysis. High degree of matching was recorded by comparing the experiment XRD exo-thione-tautomer structure parameters by their relatives DFT-optimized parameters. Moreover, the computed MEP and HSA surface interactions were compared to H-bonds and π-π stack interactions obtained by XRD-packing analyses. Docking studies reflected the compound as DNA strong hydrophobic pocket binder.

1. Introduction

Over years, 1,2,4-triazoles have been recognized as the most relevant five-membered nitrogen-containing heterocyclic due to their widespread applications in modern heterocyclic chemistry [1]. Accordingly, 1,2,4-triazole derivatives exhibited diverse fascinating properties ranging from biological to pharmacological field [2]. The most significant properties of these classes are the antioxidant, anticonvulsant, antimicrobial, anti-inflammatory, anticancer and antimalarial effects [1–8]. In addition, several clinically approved drugs such as Fluotrimazole, Ribavirin, Fluconazole, Estazolam, Alprazolam, Loreclezole and Itraconazole possess a 1,2,4-triazole core in their structures [9–11]. More significantly, some 1,2,4-triazoles tagged Schiff bases have been shown to possess remarkable antitumor, antidepressant, antimicrobial, antiviral, analgesic, antiproliferative, antituberculor antitubercular and antitumor activities [12–21].

In 1,2,4-triazole-3-thione compounds, prototropic tautomerism is highly expected since the C=S is close to the N–H group, therefore, proton transfers (thione thiol) intramigration process is detected [22–28]. Generally, proton transfers in similar systems like: DNA proton transfers, multiple proton-transfers and proton-coupled electron-transfer approaches, were computed [25]. We have recently reported the preparation of new 1,2,4-triazole-3-thione Schiff base derivative, depending on the XRD-packing result, an evidence to single proton thione thiol intramigration tautomerism was proved *via* DFT-computation [22]. Continuing these efforts, the present study accords with (i) Under MW mode of radiation, new 1,2,4-triazole derivative was prepared in excellent yield, then physicochemically analyzed, (ii) prototropic thione thiol tautomerism mechanisms *via* single and double proton transfer were DFT-computed, their transition states structures were detected by ST(Bernyl) method of calculation, (iii) DFT-optimized structure parameters were resembled with the XRD-exp. parameters,

* Corresponding author.
E-mail address: warad@najah.edu (I. Warad).

https://doi.org/10.1016/j.molstruc.2018.12.010
0022-2860/

(iv) The computed MPE and HSA calculation were compared to XRD-exp. interactions, and (v) Molecular docking of the ligand to BNA-DNA was carried out.

2. Experimental section

2.1. Materials

The chemicals were bought from Sigma Company. NMR-data was performed on 400 MHz Bruker NMR spectrometer using TMS as a reference. HR-MS was performed using an LC-MS/MS impact II. The FT-IR data were collected on SHIMADZU FTIR-8400S.

Synthesis and characterization of (E)-4-((3,4-difluorobenzylidene)amino)-2,4-dihydro-5-methyl-3H-1,2,4-triazole-3-thione.

2.2. Conventional method

(10 mmol) 4-amino-5-methyl-2,4-dihydro-1,2,4-triazole-3-thione and (30 ml) of 3,4-difluorobenzaldehyde were mixed in 50 ml ethanol as solvent and (1 ml) acetic acid. The mixture was refluxed for 6 h, the resulting precipitate was filtered after cooling, and re-crystallized from ethanol solution to afford (*E*)-4-((3,4-difluorobenzylidene)amino)-2,4-dihydro-5-methyl-3H-1,2,4-triazole-3-thione as colorless crystals in 88% yield.

2.3. Microwave method

1 mmol of 4-Amino-5-methyl-2,4-dihydro-1,2,4-triazole-3-thione, 1 mmol of 3,4-difluorobenzaldehyde, 50 ml of ethanol and 0.1 ml of acetic acid were placed in closed borosilicate vessel irradiated by MW for 5 min. Filtration and recrystallization gave (E)-4-((3,4-difluorobenzylidene)amino)-2,4-dihydro-5-methyl-3H-1,2,4-triazole-3-thione inexcellent yield (96%); m.p. 210–211 °C, FT-IR (υ, cm^{-1}): 3288 (N–H), 3120 (C-H_{ph}), 2930 (C-H_{aliph}), 1615 (C=N), 1540 (C=C), 1298 (C=S). ^{1}H NMR in DMSO-d_6, (400 MHz, ppm): δ_H 2.38 (s, 3H, C**H**$_3$), 7.60–7.67 (m, 1H, C5**H**), 7.79 (bs, 1H, C2**H**), 7.99–8.04 (m, 1H, C6**H**), 10.10 (s, 1H, **H**–C=N), 13.78 (s, 1H, N**H**). ^{13}C NMR (100 MHz, ppm) δ_C 11.16 (**C**H$_3$), 117.25 (d, 1C, $^2J_{C,F}$ = 18 Hz, **C**-5), 119.05 (d, 1C, $^2J_{C,F}$ = 18 Hz, **C**-2), 127.10 (dd, 1C, $^3J_{C,F}$ = 8 Hz, $^4J_{C,F}$ = 4 Hz, **C**-6), 130.51 (dd, 1C, $^3J_{C,F}$ = 6 Hz, $^4J_{C,F}$ = 4 Hz, **C**-1), 149.05 (H–**C**=N), 151.28 (dd, 1C, $^1J_{C,F}$ = 207 Hz, $^2J_{C,F}$ = 13 Hz, **C**-3), 153.79 (dd, 1C, $^1J_{C,F}$ = 212 Hz, $^2J_{C,F}$ = 13 Hz, **C**-4), 160.70 (**C**=N), 161.67 (**C**=S). ^{19}F NMR (377 MHz, ppm): δ_F = −136.96 to −136.84 (m, 1F, C4**F**), −132.17 to −132.05 (m, 1F, C3**F**). HRMS (ESI) m/z = 254.0438 [M^+].

2.4. XRD data

X-ray single crystal data were collected on Bruker diffractometer D8 Venture (λ = 0.71073 Å, Mo-Ka radiation) with CMOS Photon detector; the structure was solved using SHELXT and refined using SHELXL [29].

2.5. Computations

The Molecular Electrostatic Potential (MEP) was performed using the Density Functional Theory at B3LYP level of theory with 6–311 G(d,p) basis set using Gaussian09 software [30]. Hirshfeld surface analysis (HSA) and 2D fingerprint plots calculation were carried *via* d_{norm} surface property with −0.409-1.473 esu rescale using CRYSTAL EXPLORER 3.1 program [31].

3. Results and discussion

3.1. Synthesis

The targeted (*E*)-4-((3,4-difluorobenzylidene)amino)-2,4-dihydro-5-methyl-3H-1,2,4-triazole-3-thione Schiff base was made available successfully in good yield (88%), *via* classical condensation of 4-amino-5-methyl-1,2,4-triazole-3-thione with 3,4-difluorobenzaldehyde in an acetic acid medium under reflux for 6 h using ethanol as a solvent (Scheme 1). Performing the same reaction under microwave irradiation (MW) for only 5 min, reduced the reaction time and improved the yield to 96% significantly. The utility of MW as an alternative green non-conventional energy source was found to offer promising advantages as the significant reduction in the reaction time, higher products yields, high purity and greater selectivity of organic reactions [21].

Due to steric repulsion, the *exo*-isomer should be favored compared to the *endo*-one (Scheme 1) as can be seen from the results of the XRD-single analysis (see below). The product was structurally characterized based on: FT-IR, MS, CHN-analysis, XRD, ^{13}C, ^{19}F and ^{1}H -NMR. The product is soluble in polar solvents like water and alcohols and insoluble in non-polar ones as *n*-hexane.

3.2. Crystal and DFT structure analysis

The structure of (*E*)-4-((3,4-difluorobenzylidene)amino)-2,4-dihydro-5-methyl-3H-1,2,4-triazole-3-thione was analysed by X-ray diffraction. The molecule crystallizes triclinic, space group *P-1* with the following lattice parameters: a = 4.386(2) Å, b = 9.042 (5) Å, c = 14.369 (8) Å, α = 75.03 (2)°, β = 81.939 (17)°, γ = 82.14 (2)°. According to the results of the single crystal diffraction, the thione tautomeric structure was found to be favored over the thiol tautomeric one as illustrated in Fig. 1a. The C=S distance of 1.680 (16) Å demonstrates a double-bond character for this bond as indicated also by the IR and ^{13}C NMR spectra. The molecule is almost planar with dihedral angles deviating only little from 0°. The benzene ring composes a dihedral angle of 3.48° with the triazole ring indicating the exo-isomer favoured over the endo-one. Table 2 and Fig. 1b represent a comparison of the experimental structural data with those of a DFT-optimized structure.

The experimental XRD-parameters of solved structure like: bond lengths, angles and dihedral angles were compared to DFT relatives as summarized in Table 1. Both the DFT/XRD structure parameters are in the expected ranges comparable with similar systems [30,31].

Excellent harmony between XRD/DFT bond length and angle were collected as seen in the histograms Fig. 2a and Fig. 2c, respectively. R^2 = 0.979 and 0.985 graphical correlations were obtained by comparing the XRD-experimental bond lengths and angles with its DFT-theoretical values, respectively, as seen in Fig. 2b and d. Fig. 2e showed a good agreement between the XRD and DFT dihedral angles, it's very closed in its values but mostly opposite in the angles directions. By neglected the signal of dihedral angles values a strong matching between XRD/DFT was recorded.

3.3. Interactions in the crystal, MEP and HSA comparison

The existence of 4N, S, 2F and H–-N as a very polar proton in the molecule structure enhanced the formation of several short contacts [22–24]. Six types of such forces were detected per molecule in the crystal lattice which can be limited to three kinds of H-bonds and two kinds of π-π stacking interactions, as seen in Fig. 3 and Table 3.

The molecule exhibits two strong intermolecular like N–H–S as the shortest H– bonding, such bonds responsible for the inversion

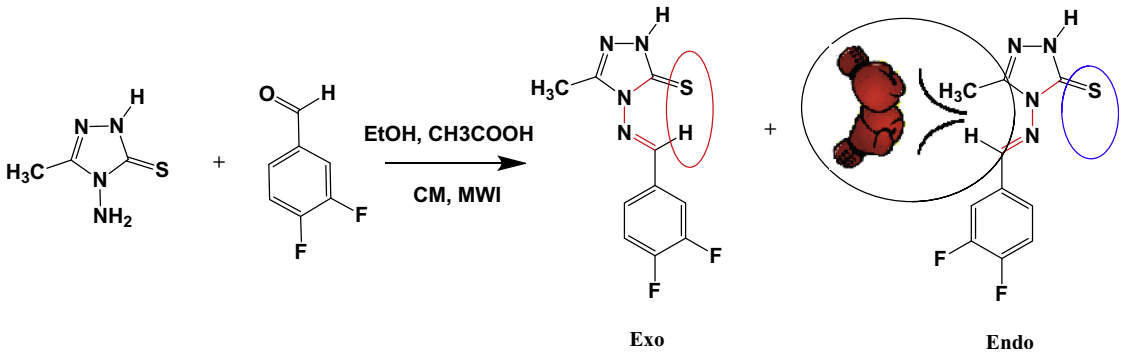

Scheme 1. Condensation reaction tautomers.

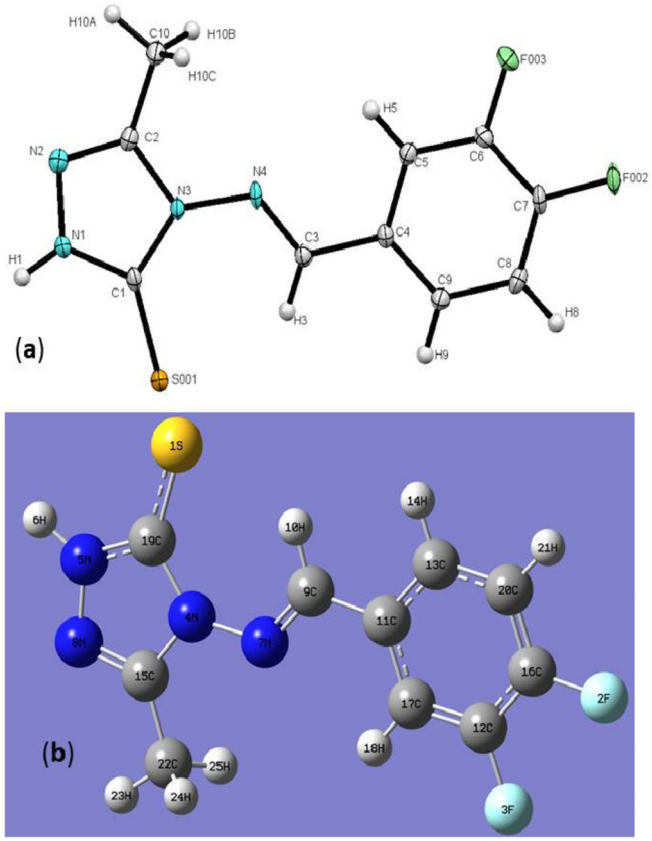

Fig. 1. (a) ORTEP and (b) DFT-optimized structures.

Table 1
Refined crystal data.

Empirical formula	$C_{10}H_8F_2N_4S$
CCDC	1824129
Formula weight	254.26
Temperature	100 K
Crystal shape, color	Needle, colorless
Space group, Crystal system	P-1 (2), Triclinic
Tmin, Tmax	0.861, 0.928
Cell dimensions	a = 4.386(2) Å α = 75.03 (2)°
	b = 9.042 (5) Å β = 81.939 (17)°
	c = 14.369 (8) Å γ = 82.14 (2)°
Volume	542.1 (5) $Å^3$
Density, Z	1.558, Mg/m^3, 2
Crystal size	0.50 × 0.06 × 0.01 mm
θ range for data collection	2.3 to 28.8 (°)
Independent reflections	5083 [R_{int} = 0.034]
R [F2>2σ], wR, S	0.033, 0.083, 1.04
Largest diff. peak and hole	0.39, −0.31 eA^{-3}

dimers of pairing molecules (Fig. 3a). The two fluoride ions with its strong electronegativity also have their contributions in H-bond formation, each molecule has four H ….F as H-bonds on form as two of $C_{Me}H$….F_{ph} and two of $C_{Ph}H$ …. F_{ph} which inverted the 2D layer shape (Fig. 3b), two N···H hydrogen bond were also cited in the lattice belongs to $C_{Ph}H$ …. N. The non-covalent π-π stacking interactions were detected as benzene to benzene centroid-to-centroid rings interactions (Fig. 3c) and the polar and shorter π(C═S) ….π(C═N) interactions (Fig. 3d), therefore, It was a reason for layer-to-layer packing formation.

The HSA computational analysis for the desired product was performed using the crystal cif file in order to figure out the expected intermolecular forces *via* red spot marked on the surface of the molecule [22–24]. Many red spots are estimated since the compound contains four heteroatoms like: F, N, S and polar H atoms. All the hydrogen bonds types were detected by HSA, big-spots were cited around the S, F and N atoms indicating such atom as strong proton accepters reflecting the formation of the shortest H-bonds (Fig. 4a–c), such seen is consistent with XRD experimental result. The π–π stacking interaction which clearly recorded by XRD packing result was not detected by HSA computed calculation. Moreover, the H to atoms percentage ratios were estimated in the desired molecule and found to be in the following arrangement: H …. .H > H …. ..F > H. ….S > H. ….N > H ….C, as seen in Fig. 4d.

The MEP computed result strongly agreed with HSA result as well as experimental XRD recorded data. MEP observed the molecule is with both electrophilic and nucleophilic positions indicated by blue and yellow colors respectively. For example, amine proton (H–N) was reflected as strong electrophilic *via* deep-blue color, the other protons like phenyl and methyl showed light blue color reflecting low electrophilic behaviors. In contrast, S, N and F atoms were detected with yellow to orange color showing nucleophilic behaviors (Fig. 5). The subsistence of H-acceptor atoms (red colors) together with H-donor sites in the molecule enhanced the H-bonds formation; such seen is consistent with the computed HSA and XRD experimentally-packing results.

3.4. Thiol thione prototropic tautomerization

Triazole-thione heterocyclic ligands excess in either thiol tautomer or thione one [22–26]. The prototropic thione thiol tautomerism proton transfer processed *via* two possible mechanisms pathways, **A**: single-proton intramigration passing through $T.S._A$ or **B:** self-assemble double proton transfer through dimer $T.S._B$,

Table 2
DFT/XRD selected bond lengths and angles result.

Bond No.	Bond type		Bond length [Å]		Angle No.	Angle type			Angle value (°)	
			XRD	DFT					XRD	DFT
1	S001	C1	1.68	1.7162	1	N4	N3	C2	117.5	118.21
2	F002	C7	1.35	1.3881	2	N4	N3	C1	133.9	133.0
3	F003	C6	1.355	1.3908	3	C2	N3	C1	108.5	108.8
4	N3	N4	1.385	1.388	4	N2	N1	C1	114.6	114.52
5	N3	C2	1.39	1.4042	5	N3	N4	C3	120.3	121.41
6	N3	C1	1.39	1.4081	6	N1	N2	C2	104.3	104.25
7	N1	N2	1.378	1.3985	7	N4	C3	C4	117	119.62
8	N1	C1	1.342	1.3603	8	C3	C4	C9	119.9	118.85
9	N4	C3	1.284	1.2966	9	C3	C4	C5	120.3	121.87
10	N2	C2	1.297	1.3131	10	C9	C4	C5	119.8	119.28
11	C3	C4	1.469	1.4629	11	F003	C6	C7	118.5	119.05
12	C4	C9	1.398	1.4064	12	F003	C6	C5	120.2	119.91
13	C4	C5	1.403	1.409	13	C7	C6	C5	121.3	121.04
14	C6	C7	1.387	1.3926	14	C4	C9	C8	120.5	120.74
15	C6	C5	1.367	1.3787	15	N3	C2	N2	110.5	110.53
16	C9	C8	1.395	1.3963	16	N3	C2	C10	123.4	123.97
17	C2	C10	1.482	1.4808	17	N2	C2	C10	126	125.51
18	C7	C8	1.376	1.385	18	F002	C7	C6	118.2	119.33
					19	F002	C7	C8	121	120.03
					20	C6	C7	C8	120.8	120.64
					21	C4	C5	C6	118.9	119.3
					22	S001	C1	N3	130.8	131.88
					23	S001	C1	N1	127	126.22
					24	N3	C1	N1	102.1	101.9
					25	C9	C8	C7	118.7	119

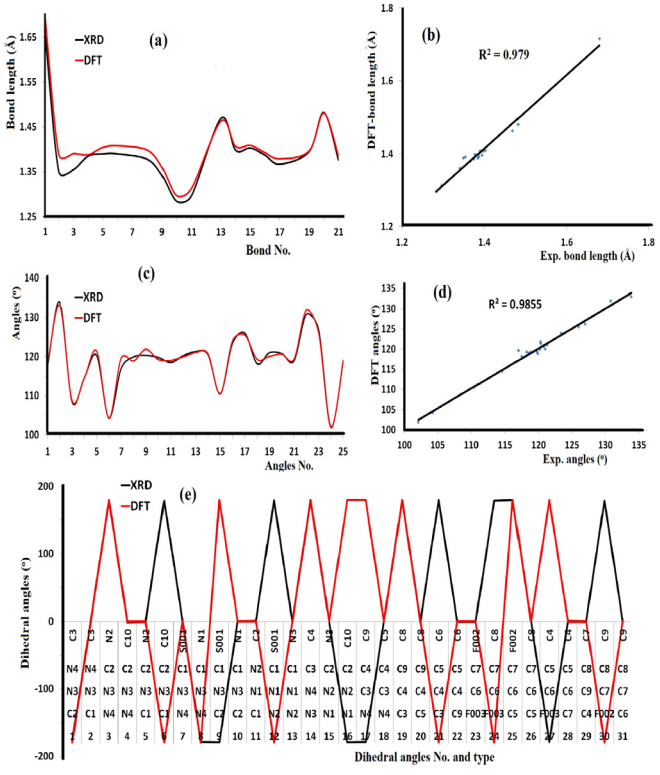

Fig. 2. (a) DFT/XRD bonds lengths histogram, (b) Graphical correlation of experimental bond lengths *vs.* DFT, (c) XRD/DFT angles histogram, (d) Graphical correlation of experimental angles *vs.* DFT ones and (e) XRD/DFT dihedral angles histogram.

as in Scheme 2. For this reason, the gas phase thiol thione tautomerization *via* both pathways have been individually computed under DFT/B3LYP/6–311 G(d,p), their transitions states were optimized using TS(Bernyl) method of calculation.

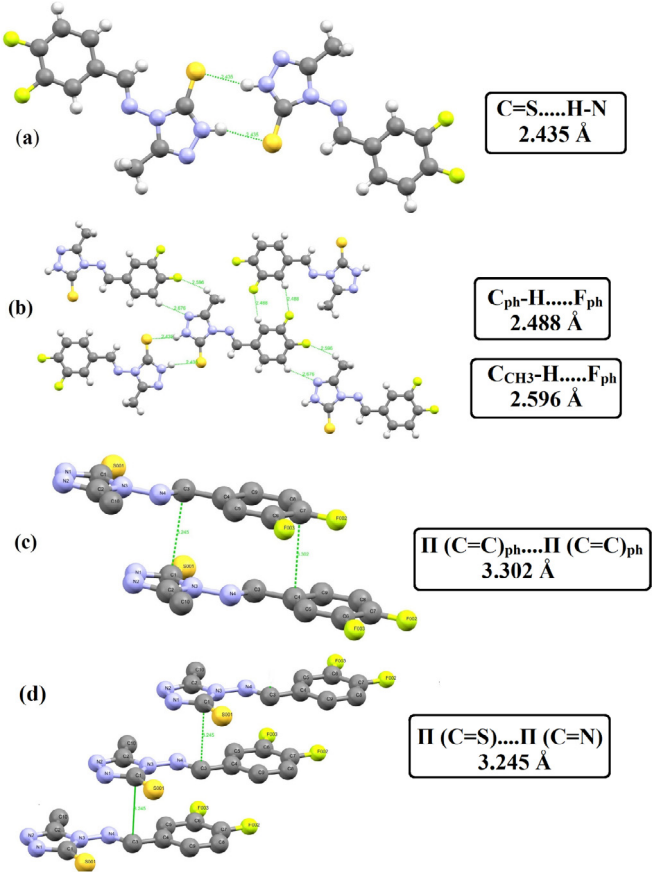

Fig. 3. Interactions lengths and types in crystal lattice.

In the prototropic thione thiol tautomerism *via* single-proton intramigration, one proton transferred from the N to the nearby S atoms through the formation of the intra-four-membered

Table 3
Short interactions in crystal lattice.

No.	Interaction type	Length Å
1	H1……S1	2.435
2	F3……H5	2.488
3	F2……H10A	2.596
4	N2……H8	2.676
5	C1……C3	3.245
6	C4……C7	3.302

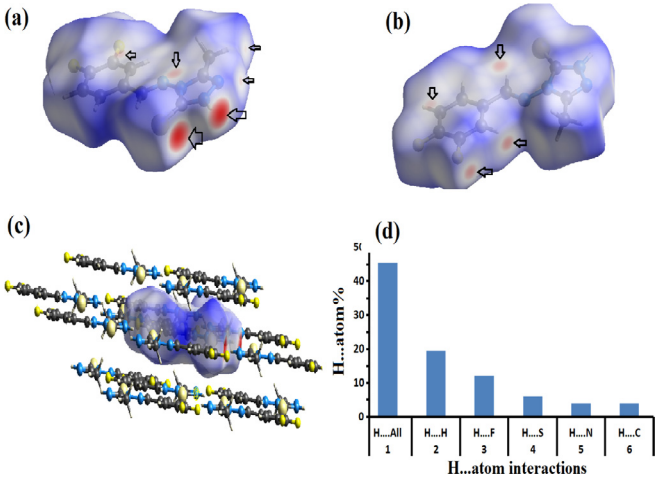

Fig. 4. (a) and (b) d_{norm} red spots with different directions, (c) layer-to-layer molecules around computed centre and (d) H … atoms fingerprint ratios.

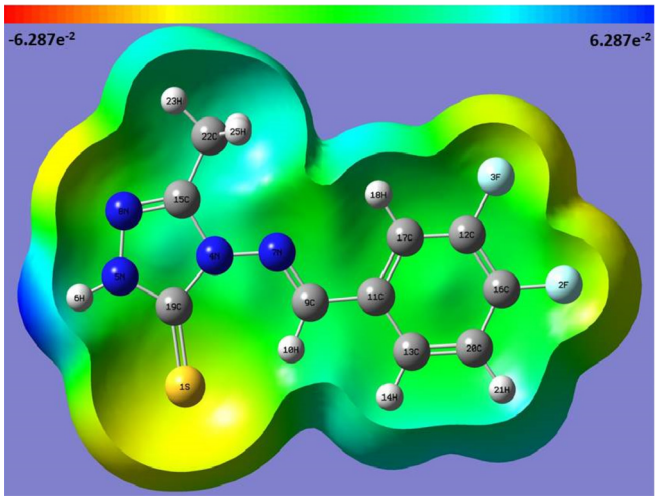

Fig. 5. (a) Molecule MEP map.

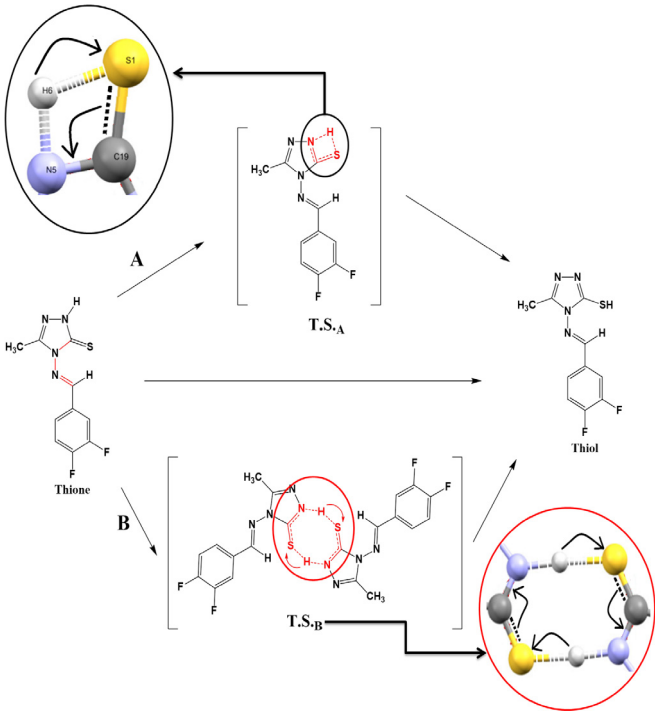

Scheme 2. Prototropic thione thiol tautomerism pathways mechanisms together with T.S's imaginary protons and π-electrons transfer.

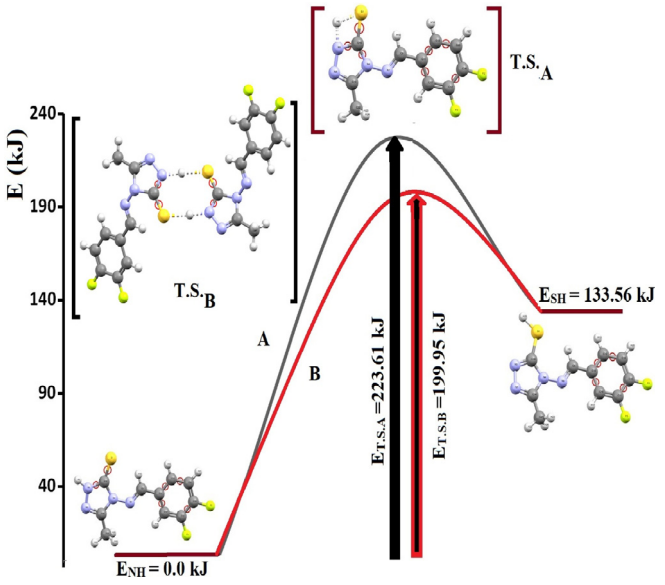

Fig. 6. Prototropic thione thiol tautomerism energy profiles.

transition state ring with S1···H1 and N1···H1 distances of 1.710 and 1.464 Å, respectively (Scheme 2 and Fig. 6). Such gaseous-phase proton transfer transition state ($T.S._A$) reflected an imaginary vibrational frequency with 1481i cm^{-1}, which consistent with proton intramigration reported processes [22–28].

In self-assembly double proton transfer *via* dimer formation, two protons were transferred after a possible self-assembly of two molecules of the title compound to form the dimer as in Scheme 2 and Fig. 6; such suggestion was supported by the XRD-experimental background result reported in Fig. 3a, to understanding such protons move father, herein, the process of self-assemble double proton transfer dependent on proton push and proton pull principle have been investigated, the two protons are transferred in opposite direction concertedly the dimer-assisted proton movement from molecule to the next one versa vista at, it's like taking a proton and giving another at the same time and speed reflecting the transition state ($T.S._B$) with S1···H1 and N1···H1 bond distances of 1.965 and 1.450 Å, respectively. For the $T.S._B$, the symmetrical imaginary vibrational frequency was recorded at 1691i cm^{-1} while the asymmetrical one found to be at 1237i cm^{-1}, the presence of more the one imaginary vibrational is consistent strongly with double proton exchange process [26].

Gaseous-energy profiles of both prototropic thione thiol tautomerism *via* minimum energy principle reflected the self-assemble double proton transfer with less energy transition state. The $E_{T.S.B}$ computed to 199.95 kJ/mol, while the single-proton intramigration processed with $E_{T.S.A} = 223.61$ kJ/mol, as illustrated in Fig. 6. This seen in not suppressing to us since the dimer-molecule structure was detected by XRD-solid state packing analysis. Even in this case, the difference in transition states energy of both mechanisms is less than 25 kJ/mol, we still believe that the reaction in gaseous state favored to process *via* double proton transfer mechanism more than single proton one, since this suggestion is supported with the solid state XRD-seen.

3.5. Experimental and theatrical ^{19}F, ^{1}H and ^{13}C NMR

The experimental ^{19}F NMR spectrum displayed two characteristic multiplets signal at δ_F −136.96 to −136.84 ppm and −132.17 to −132.05 ppm, consistent with the two signals of DFT/B3LYP6-311 + G(2d,p) GIAO ^{19}F NMR reflecting the presence of two aromatic fluorine atoms in the thione tautomer (Fig. 7a). The thione-Schiff base tautomer was supported over the thiol one also by ^{1}H NMR analysis, the triazolyl N–H acidic proton manifested as a broad-singlet with a downfield chemical shift at δ_H 13.78 ppm. Moreover, the appearance of a new distinct singlet of the imine proton (H–C=N) at δ_H 10.10 ppm confirmed the condensation reaction completeness. The spectrum also displayed one singlet belongs to CH_3 protons at δ_H 2.37 ppm and three phenyl signals at δ_H 7.60–8.04 ppm. The computed DFT/B3LYP6-311 + G(2d,p) GIAO ^{1}H NMR is in agreement with experimental as seen in Fig. 7b, a graphical correlation R^2 with 0.9952 was recorded when both DFT/Exp. ^{1}H NMR are compared. ^{13}C NMR also support thione-Schiff base tautomer formation *via* the occurrence of a downfield distinct signal at δ_C 173.41 attributed to C=S carbon. The spectrum also displayed additional resonances at δ_C 11.16 and 160.70 ppm assigned to the CH_3 and azomethine (C=N) carbons, respectively. The aromatic carbons were recorded at their classical positions within $\delta_C = 117.25–153.79$ ppm as two doublets and four doublets due to the fluorine-carbon coupling effect (Fig. 7c).

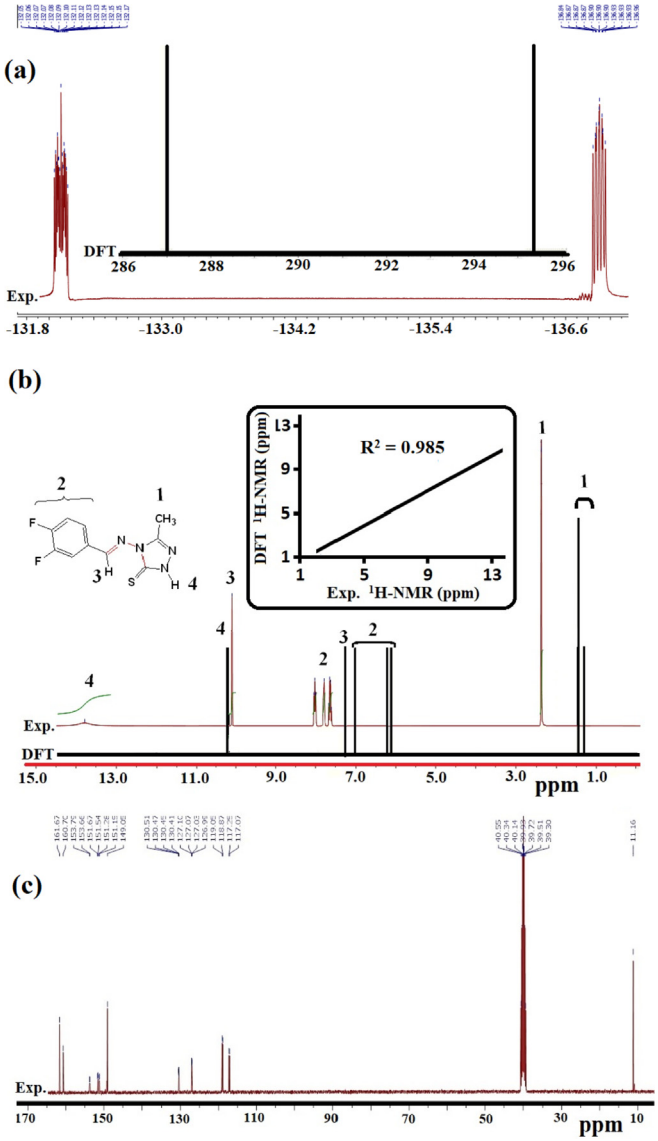

Fig. 7. Exp./theoretical NMR data (a) ^{19}F, (b) ^{1}H and (c) ^{13}C in DMSO-d_6.

3.6. IR spectrum

The FT-IR spectrum of the desired thione Schiff base reflected several functional groups vibration as recorded in Fig. 8a, the experimental result was supported by DFT-computational analysis (Fig. 8b). Good agreement with R^2 graphical correlation = 0.9952 was observed by comparing DFT with exp. IR result, as seen in Fig. 8c. The main characteristic absorptions vibrations are illustrated as exp. and DFT, respectively: $\upsilon_{N-H} = 3288$ and 3700 cm^{-1}, $\upsilon_{(C-H)ald} = 3120$ and 3280 cm^{-1}, $\upsilon_{(C-H)ph} = 3080$ and 3150 cm^{-1}, $\upsilon_{(C-H)\ aliph} =$ and 3060 cm^{-1}, $\upsilon_{C=N} = 1615$ and 1640 cm^{-1}, $\upsilon_{C=S} = 1298$ and 1320 cm^{-1}, therein $\upsilon_{C=S}$ vibration clearly supported thione-Schiff base tautomer formation over thiol-one, as seen Fig. 8.

3.7. Hydrophobic pocket docking analysis

Due to the high binding energy (7.9 kcal/mol) stimulated from Ligand:DNA complex molecular docking results. Theoretically, the compound can be classified as strong DNA-binder with high binding constant $K_b = 1.2 \times 10^6$. Moreover, the surface representation showed that the compound was impeded totally in between the DNA-double helix, as seen in Fig. 9a, but it is very important to note that no forces like H-bonds, electrostatic, π-π stacking, along with other non-covalent interactions where detected *via* auto-docking of the ligand with the DNA (Fig. 9b). Meanwhile, many H-bonds together with π-π stacking interactions were detected in the crystal lattice of the ligand (see Fig. 3).

Therefore, hydrophobic pocket with tight fit interactions can be

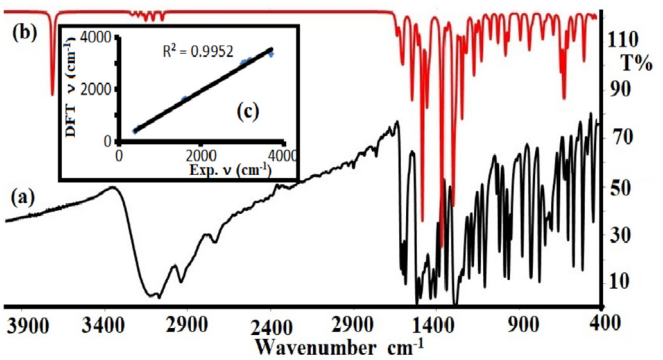

Fig. 8. FT-IR: (a) Experimental, (b) DFT and (c) DFT/Exp. graphical correlation.

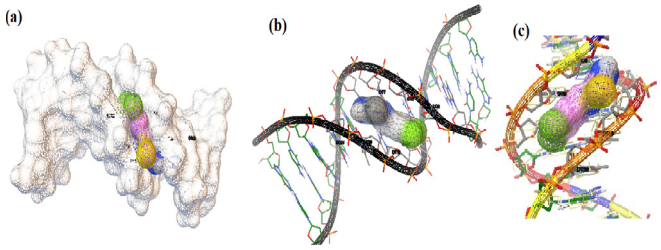

Fig. 9. [BNA-Ligand] hydrophobic pocket interaction (a) double helix binding schematic representation (b) Minor groove pocket position interactions (c) Nuclides pocket around ligand.

suggested, whereas, the ligand is planar in geometry with sp^2-hybridizations atoms (except the phenylic CH_3), in addition, the ligand is high polar since several polar functional groups constructed its backbone. These advantages reflected the compound as good minor groove penetrator, therefore, pocket interactions can be formed [32–34], were the ligand is surrounding by several nuclides such as; DG10, DC9, DT8, DT7, DA17, DA18, DT19 and DT20, as seen in Fig. 9c.

4. Conclusions

With an excellent yield, new fluorinated triazole Schiff base derivative was made available under MW mode of vibration. Only thione tautomer has been isolated and its exo structure was supported by XRD-single analysis. The prototropic thione thiol computational tautomerism reaction *via* self-assemble double proton transfer was found to be favored over the single-proton intramigration mechanism process. The structure was characterized based on MS, FT-IR, CHN-EA, ^{19}F, ^{1}H, and ^{13}C NMR. Moreover, the comparison of computed/experimental structural data, NMR, IR data belongs to the compound reflected an excellent degrees of compatibility. The computed MPE and HSA result detected the existence of various short types of H-bonds and π-π stacks interactions which experimentally were confirmed by XRD-crystal packing analysis. Novel hydrophobic pocket interactions with high binding constant $K_b = 1.2 \times 10^6$ was recorded *via* docking the compound with the DNA.

Acknowledgements

Musa A. Said is thankful to Alexander von Humboldt for the continuous support.

References

[1] N. Bulut, U.M. Kocyigit, I.H. Gecibesler, T. Dastan, H. Karci, P. Taslimi, S. Durna Dastan, I. Gulcin, A. Cetin, J. Biochem. Mol. Toxicol. 32 (2018) 22006–22012.
[2] T. Plech, B. Kaproń, J.J. Łuszczki, A. Paneth, A. Siwek, M. Kołaczkowski, M. Żołnierek, G. Nowak, Eur. J. Med. Chem. 86 (2014) 690–699.
[3] H.A. Saadeh, I.M. Mosleh, A.G. Al-Bakri, M.S. Mubarak, Monatshefte Für Chem.-Chem. 141 (2010) 471–478.
[4] M.R. Aouad, M.M. Mayaba, A. Naqvi, S.K. Bardaweel, F.F. Al-blewi, M. Messali, N. Rezki, Chem. Cent. J. 11 (2017) 117–127.
[5] G.A.A. Abuo-Rahma, M. Abdel-Aziz, E.A.M. Beshr, T.F.S. Ali, Eur. J. Med. Chem. 71 (2014) 185–198, 1,2,4.
[6] S.R. Patil, A. Asrondkar, V. Patil, J.N. Sangshetti, F.A. Kalam Khan, M.G. Damale, R.H. Patil, A.S. Bobade, D.B. Shinde, Bioorg. Med. Chem. Lett 27 (2017) 3845–3850.
[7] A. Ahmad, H. Varshney, A. Rauf, A. Sherwani, M. Owais, Arab. J. Chem. 10 (2017) S3347–S3357.
[8] M. Asif, Int. J. Adv. Res. Chem. Sci. 1 (2014) 2349–2403.
[9] V. Merck, in: M. O'Neil, A. Smith, P.E. Heckelman, S. Budavari (Eds.), The Merck Index. An Encyclopedia of Chemicals, Drugs and Biologicals, an Encycl. Chem. Drugs Biol. Merck Index, fifteenth ed., Merck Co., Inc. White House Station., Hunterdon, NJ, USA, 2001, 320 and 3737.
[10] C. Hart, Mod. Drug Discov. 2 (1999) 20–31.
[11] R.W. Sidwell, L.B. Allen, J.H. Huffman, J.T. Witkowski, L.N. Simon, Exp. Biol. Med. 148 (1975) 854–858.
[12] G.-Q. Hu, X.-L. Dong, S.-Q. Xie, W.-L. Huang, Acta Pharm. Sin. 43 (2008) 50–53.
[13] F. Clerici, D. Pocar, M. Guido, A. Loche, V. Perlini, M. Brufani, J. Med. Chem. 44 (2001) 931–936.
[14] A.A. Shanty, J.E. Philip, E.J. Sneha, M.R. Prathapachandra Kurup, S. alachandran, P.V. Mohanan, Bioorg. Chem. 70 (2017) 67–73.
[15] M. Mesbah, T. Douadi, F. Sahli, S. Issaadi, S. Boukazoula, S. Chafaa, J. Mol. Struct. 1151 (2018) 41–48.
[16] K.S. Kumar, S. Ganguly, R. Veerasamy, E. De Clercq, Eur. J. Med. Chem. 45 (2010) 5474–5479.
[17] A. Barakat, M.S. Islam, A.M. Al-Majid, H.A. Ghabbour, S. Atef, A. Zarrouk, I. Warad, J. Theor. Comput. Chem. 17 (2018) 1850005–1850028.
[18] N. Rezki, A. Al-Yahyawi, S. Bardaweel, F. Al-Blewi, M. Aouad, Molecules 20 (2015) 16048–16067.
[19] T. Aboul-Fad, F.A.S. Bin-Jubair, O. Aboul-Wafa, Eur. J. Med. Chem. 45 (2010) 4578–4586.
[20] K. Zhang, P. Wang, L.-N. Xuan, X.-Y. Fu, F. Jing, S. Li, Y.-M. Liu, B.-Q. Chen, Bioorg. Med. Chem. Lett 24 (2014) 5154–5156.
[21] D.A. Sabbah, F. Al-tarawneh, W.H. Talib, K. Sweidan, S.K. Bar, Med. Chem. 14 (2018) 1–14.
[22] M.R. Aouad, M. Messali, N. Rezki, N. Al-Zaqri, I. Warad, J. Mol. Liq. 264 (2018) 621–630.
[23] S.B. Benaka Prasad, S. Naveen, C.S.A. Kumar, N.K. Lokanath, A.V. Raghu, I. Daraghmeh, K.R. Reddy, I. Warad, J. Mol. Struct. 1167 (2018) 215–226.
[24] S. Tabti, A. Djedouani, D. Aggoun, I. Warad, S. Rahmouni, S. Romdhane, H. Fouzi, J. Mol. Struct. 1167 (2018) 215–226.
[25] E.H. El Ashry, L.F. Awad, S.M. Soliman, M.N.A. Al-Moaty, H.A. Ghabbour, A. Barakat, J. Mol. Struct. 1146 (2017) 432–440.
[26] N. Özdemir, D. Türkpence, Comput. Theor. Chem. 1025 (2013) 35–45.
[27] N.B. Arslan, N. Özdemir, O. Dayan, N. Dege, M. Koparır, P. Koparır, H. Muğlu, Chem. Phys. 439 (2014) 1–11.
[28] N. Burcu Arslan, Namık Özdemir, J. Mol. Model. 21 (2015) 19–29.
[29] G.M. Sheldrick, Acta Crystallogr. Sect. C Struct. Chem. 71 (2015) 3–8.
[30] S.K. Wolff, D.J. Grimwood, J.J. McKinnon, D. Jayatilaka, M.A. Spackman, Crystal Explorer 2.1, University of Western Australia, Perth, 2007.
[31] M.J. Frisch, G.W. Trucks, et al., Gaussian 09, Gaussian Inc., Wallingford CT, 2009.
[32] S. Veeralakshmi, G. Sabapathi, S. Nehru, P. Venuvanalingam, S. Arunachalam, Colloids Surfaces B Biointerfaces 153 (2017) 85–94.
[33] H. Fu, K. Zheng, M. Zhang, Y. Li, Z. Wu, C. Yan, J. Photochem. Photobio B: Biology 161 (2016) 80–90.
[34] E. Philot, D. Perahia, A. Braz, M.S. Costa, L. Scott, J. Struct. Biol. 184 (2013) 293–300.